RSC Advances

PAPER

View Article Online
View Journal | View Issue

Cite this: *RSC Adv.*, 2014, **4**, 19716

Organic hydroperoxide formation in the acid-catalyzed heterogeneous oxidation of aliphatic alcohols with hydrogen peroxide†

Qifan Liu, Weigang Wang,* Ze Liu, Tianhe Wang, Lingyan Wu and Maofa Ge*

Received 21st March 2014
Accepted 7th April 2014

DOI: 10.1039/c4ra02486a

www.rsc.org/advances

Organic hydroperoxides (ROOH) are reactive species which play significant roles in atmospheric processes, such as acid precipitation, hydroxyl radical cycling and secondary organic aerosol formation. Despite their observation in the atmosphere, our understanding of their formation mechanism is still incomplete. In the present work, ROOH formation was found in the acid-catalyzed heterogeneous oxidation of aliphatic alcohols with hydrogen peroxide. The kinetics and mechanism of acid-catalyzed heterogeneous oxidation of three aliphatic alcohols (2-methyl-2-butanol, 3-buten-2-ol and 2-butanol) with hydrogen peroxide were investigated. Based on the experimental results, tertiary or allyl alcohols may contribute to ROOH formation through this route while secondary alcohols may not. The kinetic experiments were conducted in a rotated wetted-wall reactor coupled to a mass spectrometer at room temperature (298 K) with 40–70 wt% H_2SO_4 solution. The reactive uptake coefficients were acquired for the first time. The generation and degradation mechanisms of ROOH in acidic media were proposed according to the product information. Once formed, ROOH are found to undergo two degradation pathways: the acid-catalyzed rearrangement reaction and the organic hydrogen peroxysulfate formation pathway. The newly found acid-catalyzed process may occur under certain conditions and influence particle growth in the atmosphere.

Introduction

Organic hydroperoxides (ROOH) play significant roles in the atmosphere due to their multiple roles as oxidants and reservoirs of radicals.[1,2] Moreover, they are considered to be important species of secondary organic aerosol (SOA) and have negative impacts on vegetation.[3–5] A series of ROOH, including methyl hydroperoxide (MHP), hydroxymethyl hydroperoxide (HMHP), and ethyl hydroperoxide (EHP) have been measured in the atmosphere.[6–8] Nowadays, it is believed that three reaction pathways may contribute to the formation of ROOH. The bimolecular reaction between organic peroxy radicals (RO_2) and hydroperoxyl radicals (HO_2) is the first route.[9] The second one is the ozonolysis reaction of alkenes.[9,10] The third pathway involves reversible addition of hydrogen peroxide (H_2O_2) to aldehydes.[11] Here, we propose a new route through oxidation with H_2O_2 under acidic conditions that may result in ROOH formation from aliphatic alcohols.

Aliphatic alcohols (ROH), an important class of volatile organic compounds, are emitted into the atmosphere by different natural and anthropogenic sources.[12,13] It could be highly abundant in certain regions, for example, high rates of emission of 2-methyl-3-buten-2-ol (MBO) were measured from pine species in western United States.[14–16] It is well recognized that H_2O_2 plays a vital role in both aqueous-phase and gas-phase oxidation.[17] H_2O_2 was observed in cloud water with the concentration ranging from 37.8 μM to 283.2 μM,[18] and was expected to be present in fine particles at a concentration of 0.1–1mM.[19] On the basis of filter extracts of ambient aerosols and model calculations, Arellanes *et al.*[20] suspected that H_2O_2 concentration in aerosol liquid water might be up to 70 mM. Previous field observations and experimental studies[21–23] have revealed that acid-catalyzed particle-phase reactions of biogenic volatile organic compounds (for example, isoprene and terpenes) or their reactive oxidation products (for example, epoxides) provide a potential source for SOA. Laboratory experiments have also suggested that acid-catalyzed heterogeneous oxidation of isoprene with H_2O_2 makes a contribution to SOA formation.[24,25] Given the cloud water samples collected from field measurements were often acidic[26,27] and the estimated pH of liquid aerosol droplets was on the order of −0.8 to 1.18 in northeastern United States,[28] heterogeneous reactions of ROH and H_2O_2 in acidic media may take place under certain atmospheric conditions. Previous studies of ROH (for example,

Beijing National Laboratory for Molecular Sciences (BNLMS), State Key Laboratory for Structural Chemistry of Unstable and Stable Species, Institute of Chemistry, Chinese Academy of Sciences, Beijing, 100190, P. R. China. E-mail: wangwg@iccas.ac.cn; gemaofa@iccas.ac.cn; Tel: +86-10-62558682; +86-10-62554518

† Electronic supplementary information (ESI) available. See DOI: 10.1039/c4ra02486a

methanol, butanol, decanol and MBO) mainly focus on their heterogeneous interactions with sulfuric acid (H_2SO_4) because of their high activities to form organosulfates,[29–32] these reactions may contribute to aerosol growth. However, the heterogeneous chemistry between ROH and H_2O_2 in acidic media remains largely uncertain. To the best of our knowledge, little attention is paid on the heterogeneous oxidation of ROH with H_2O_2 in the presence of H_2SO_4, especially a systematic study of heterogeneous interactions between different structures of ROH and H_2O_2 in acidic media is still lacking. Hence, the acid-catalyzed heterogeneous reactions of three different structures of ROH (2-methyl-2-butanol, 3-buten-2-ol and 2-butanol), representing tertiary, allyl and secondary alcohols, respectively, were investigated in this study. The purpose of this research is to gain more knowledge about the uptake kinetics and corresponding chemical mechanisms of diverse structures of ROH into H_2SO_4–H_2O_2 mixed solution. ROOH, organic peroxides (ROOR) and organosulfates were found to be produced by the heterogeneous process.

Experimental section

Uptake measurements

The uptake measurements were conducted in a rotated wetted-wall (RWW) flow tube reactor coupled to a signal-photon ionization time of flight mass spectrometer (SPI-TOFMS), similar to our previous study.[33] Briefly, it is a reactor consisted of a Pyrex tube with a glass jacket for thermostatic control. A rotating cylinder (length $L = 30$ cm, inner radius $R = 1.25$ cm, rotating rate $r = 10$–15 rpm) was put into the Pyrex tube, holding small volume of solutions (about 3.5 mL) to form liquid film (about 0.15 mm thickness) evenly on the inner wall. A glass stirring bar was placed on the bottom of the cylinder to ensure that the solution could be mixed and spread sufficiently. To avoid the change of solution composition during one experimental period of time, a mixture of helium (He) and water vapor in equilibrium with the solution was used as carrier gas. Reactant gas was introduced into the reactor at a small flow rate (ten percent of the carrier gas) through a movable glass injector ($D =$ 6 mm) which was centered in the rotating cylinder. This glass injector allowed for the variation of the contact time between the solution and reactant gas. Typically, the total pressure was in the range of 5.9 to 24.0 Torr and the reactant concentration in the reactor was on the order of 4.8×10^{14} to 1.9×10^{15} molecules per cm^3. All of the experiments were carried out at the room temperature (298 K). The Reynolds number calculated was smaller than 2000 under our experimental condition. In this situation, the measurements were operated under the approximate laminar flow condition. Details of SPI-TOFMS are described in the ESI.†

Reactive uptake coefficient (γ)

As an uptake experiment just began, the movable injector was placed at the zero position and the solution was unexposed. In this situation, the unperturbed mass signal of reactant gas can be recorded as baseline S_0. Then the injector was pulled upstream to expose the solution to the reactant gas and the signal dropped down simultaneously. Reactive uptake was indicated by a constant offset between the original signal S_0 and the reactive uptake signal with time, S. The observed first-order rate constant for removal of the reactant gas from gas-phase, k_{obs} (s^{-1}) can be calculated from eqn (1):

$$\ln\left(\frac{S}{S_0}\right) = -k_{obs}\frac{L}{v_{ave}} \quad (1)$$

where v_{ave} (cm s^{-1}) is the average gas flow velocity of the reactant gas, and L (cm) is the contact distance of the solution and reactant gas. k_{obs} can be determined more accurately by placing the injector at various positions in the reactor to change the contact distance. Fig. S1a† depicts the loss of 2-butanol signal as a function of injector position. The rate constant for removal of the reactant gas, $k_{gas-liquid}$ (s^{-1}), can be determined by correcting k_{obs} for diffusion:[34,35]

$$\frac{1}{k_{gas-liquid}} = \frac{1}{k_{obs}} - \frac{1}{k_{diff}}\left(k_{diff} = \frac{3.66D_i}{r^2}\right) \quad (2)$$

where D_i (cm^2 s^{-1}) is the diffusion coefficient which can be calculated from the Huller–Schettler–Gidding method,[36] r (cm) is the inner radius of the rotating cylinder, and k_{diff} is the diffusion-limited rate (s^{-1}). Finally, the γ can be acquired from eqn (3):

$$\gamma = \frac{4k_{gas-liquid}V}{\omega A} \quad (3)$$

where V (cm^3) is the volume of the reaction zone, A (cm^2) is the geometric area of the exposed solution, and ω (m s^{-1}) is the mean molecular speed of reactant alcohol. More calculation details are shown in the ESI.†

Gas-phase products identification

To further survey the gas-phase products, off-line FTIR spectrometer experiments were performed. The gas-phase species were collected in a U-shape collector located in a liquid nitrogen bath and then analyzed by FTIR spectrometer (Nicolet 6700, Thermo Scientific). The IR spectra provide information about the groups of the products molecules in the spectral range from 650 to 4000 cm^{-1}.

Aqueous–phase reactions

Aqueous-phase reactions of ROH (2-butanol, 2-methyl-2-butanol, *tert*-butyl alcohol and 3-buten-2-ol) and H_2SO_4–H_2O_2 mixed solution were performed to further study the mechanism. Mixture of 0.1 mL ROH and 5 mL H_2SO_4 (or H_2SO_4–H_2O_2 mixed solution) were shaken thoroughly at 298 K for 2 h before analysis. Then the mixture was extracted by 2 mL dichloromethane (CH_2Cl_2). To further investigate the formation mechanism of ROOH, 200 mg 2 wt% $H_2{}^{18}O_2$ was added into *tert*-amyl sulfate (TAS) solution, which was prepared by the reaction of 40 mg 2-methyl-2-butanol and 200 mg H_2SO_4 (0.2 M). Another reaction between 40 mg 2-methyl-2-butanol and 400 mg H_2SO_4 (pH = 1)–$H_2{}^{18}O_2$ (1 wt%) mixed solution was also conducted. The mixture was extracted by CH_2Cl_2 after 2 h reaction. Only the

organic-phase after extraction was analyzed by GC-MS and ESI-MS because a large amount of H_2SO_4 remained in the water-phase, hindering the detection of products signals. The pH of the reaction mixture was around 1. This acidity is relevant to the measured range of acidity in atmospheric aerosols.[28] As for H_2O_2, we assume 70 mM to be its upper limit in the atmosphere according to previous work.[20] 0.1 wt% H_2O_2 (about 30 mM) solutions were used in the uptake measurements and higher concentration (1 wt%) of H_2O_2 solutions were used to investigate the mechanism readily. As for the aqueous-phase reactions, considering a certain loss of products in the water-phase, the limit of detection for GC-MS and ESI-MS, high concentration of H_2O_2 (10 mM and 300 mM) solutions were used during the experiments. GC-MS analysis, ESI-MS analysis and the chemicals used in these experiments are described in the ESI.†

Results and discussion

Uptake behaviors and kinetics

Uptake measurements were performed by exposing the gaseous alcohols to a certain length of the H_2SO_4 solution and monitored the MS-signal change meanwhile. Fig. 1 depicts the temporal profiles of 2-butanol signals during the uptake measurements. As the H_2SO_4 concentration increased, the uptake behavior of 2-butanol changed from reversible to irreversible. For 50 wt% H_2SO_4 solution, the signal dropped instantly upon exposure and returned to its original level as the solution was saturated. Pushing the injector back to its initial position produced an opposite change in signal, corresponding to the release of 2-butanol back to the gas-phase. The similarity in shape and total area of the adsorption and desorption curves implied the occurrence of reversible uptake. For 70 wt% H_2SO_4 solution, the uptake displayed a steady-state feature and exhibited no saturation on the time scale of the experiment, indicating that irreversible reactions dominated the uptake process. In a number of experiments, partially irreversible uptake were observed in the variation of the signal (Fig. 1b): 2-butanol was found to be taken up and released at a later time, but additionally a constant signal offset was observed. The similar cases were also reported in previous publications.[30,31] Absorption and desorption likely explain the reversible uptake, the formation of organosulfates and dehydration process could account for the irreversible uptake. For the partially irreversible uptake, a part of gaseous alcohol molecules are physically absorbed while the others could undergo irreversible reactions. The uptake behavior of 3-buten-2-ol was similar with that of 2-butanol. For 2-methyl-2-butanol, reversible uptake was observed for the solution with H_2SO_4 concentration below 40 wt %. The partially irreversible uptake occurred for the 50–60 wt% H_2SO_4 and the uptake on 70 wt% H_2SO_4 was totally irreversible. When adding H_2O_2 into H_2SO_4 solution, the steady-state uptake of 2-methyl-2-butanol and 3-buten-2-ol occurred at a lower acidity while the uptake behavior of 2-butanol stayed unchanged.

Table 1 summarizes the γ of these three compounds and the corresponding experimental conditions are listed in Table S1.† It seems that H_2O_2 plays a role in the enhancement of γ for

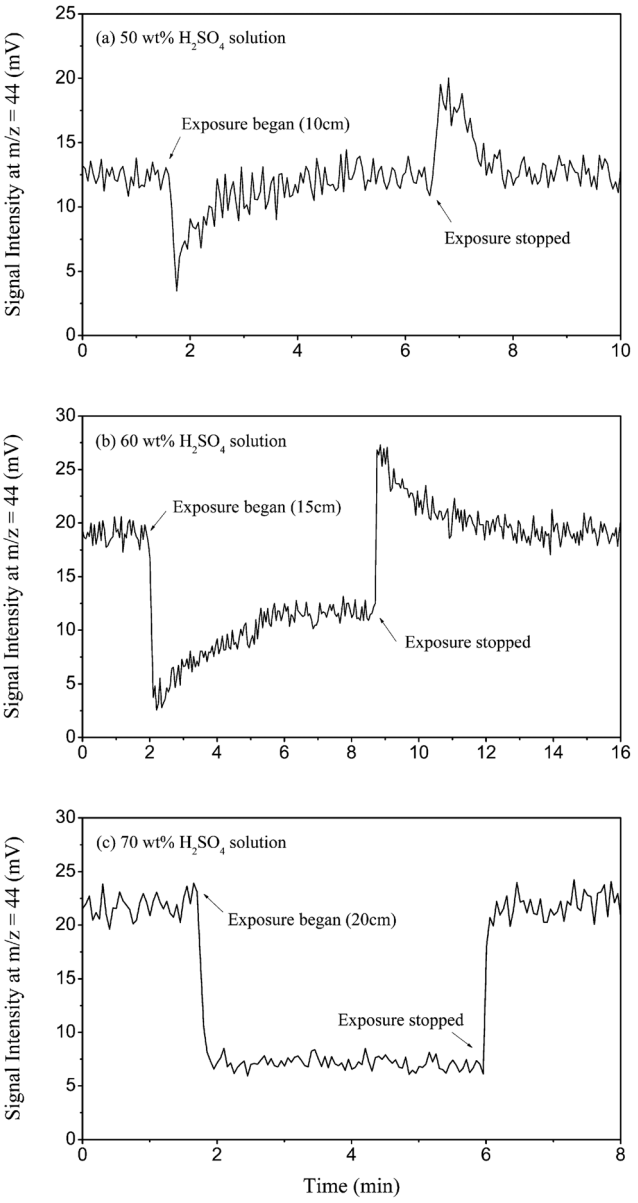

Fig. 1 Typical experimental profiles of 2-butanol. (a) reversible uptake into 50 wt% H_2SO_4 solution; (b) partially irreversible uptake into 60 wt% H_2SO_4 solution; (c) irreversible uptake into 70 wt% H_2SO_4 solution.

2-methyl-2-butanol and 3-buten-2-ol, but has little impact on the uptake of 2-butanol. As for reactive gas uptake, Davidovits *et al.*[37] have suggested that the chemical reactions mainly contribute to the uptake process in many cases. Different chemical mechanisms could be used to explain the diverse uptake behaviors of these compounds. The reactions between ROH and H_2SO_4 at the surface or in the bulk liquid involve two process: dehydration pathway and the formation of organosulfates. When exposing gaseous ROH to H_2SO_4–H_2O_2 mixed solution, a different route that produces ROOH is found except for the reaction of 2-butanol. These reactions are described in detail in the following section. Increasing acidity could result in faster reactions for all three alcohols, thus leading to the enhancement of γ. More concentrated H_2O_2 also accelerates the

Table 1 Summarization of reactive uptake coefficients for three aliphatic alcohols[a]

Gas reactant	H_2SO_4 (wt%)	H_2O_2 (wt%)	$\gamma^{\dagger}$ ($\times 10^{-4}$)
2-Butanol	60	0	0.98 ± 0.02
	60	1	0.82 ± 0.01
	70	0	1.98 ± 0.05
	70	1	2.01 ± 0.04
2-Methyl-2-butanol	40	0	—
	40	1	0.46 ± 0.02
	50	0	0.27 ± 0.02
	50	0.1	0.51 ± 0.16
	50	0.5	2.21 ± 0.15
	50	1	5.89 ± 0.12
	60	0	1.99 ± 0.04
	60	0.1	2.93 ± 0.02
	60	0.5	5.65 ± 0.15
	60	1	18.43 ± 1.09
	70	0	12.52 ± 0.68
	70	0.1	16.00 ± 0.03
	70	0.5	29.63 ± 0.62
	70	1	66.49 ± 0.64
3-Buten-2-ol	50	0	—
	50	1	1.61 ± 0.13
	60	0	1.10 ± 0.07
	60	0.1	1.28 ± 0.04
	60	0.5	1.57 ± 0.04
	60	1	7.60 ± 0.37
	70	0	2.21 ± 0.44
	70	0.1	2.57 ± 0.07
	70	0.5	3.93 ± 0.16
	70	1	17.13 ± 0.32

[a] — represents no obvious uptake. † Each value is the average of at least three measurements, and the error corresponds to one standard deviation (σ).

reaction rates except for that of 2-butanol. The γ of these three alcohols under the same experimental conditions (same H_2SO_4 and H_2O_2 concentration) are found to follow the sequence: 2-methyl-2-butanol > 3-buten-2-ol > 2-butanol. The generation of carbocation could be a key step either in the dehydration process or the formation of organosulfates and ROOH.[38] The stability of carbocations formed during the reactions likely determines the reaction rates which follow the sequence: tertiary > allyl > secondary carbocation. Hence, if the carbocation formation is the central process, it is reasonable that the value of γ for 2-methyl-2-butanol is the biggest among these three alcohols under the same conditions.

Products identification

For the uptake of 2-butanol into 70 wt% H_2SO_4 solution (Fig. S1b†), reactant signals (m/z = 44, 45, 59 and 74) dropped down as soon as gaseous 2-butanol was exposed to H_2SO_4 solution, meanwhile a new peak at m/z = 56 was detected from the mass spectrum. This peak is ascribed to (*E*)-2-butene formed through the dehydration of 2-butanol, which is confirmed by the gas-phase products analysis using FTIR spectroscopy (Fig. S2b†). This result coincides with the Zaitsev's rule (see the ESI† for more details). Aqueous-phase reactions were performed to further survey the products. Fig. S3a† shows the ESI-MS spectrum (in the negative mode) of extracted organic-phase from aqueous-phase reactions between 2-butanol and H_2SO_4 (pH = 1). The peak at m/z = 153 ($C_4H_9SO_4^-$) represents the signal of 1-methylpropyl sulfate. Organosulfates were common products formed through this pathway, which were also observed in previous studies.[29–32] These results indicate that heterogeneous reactions of 2-butanol and H_2SO_4 could result in (*E*)-2-butene and organosulfates formation.

A new peak at m/z = 70 appeared in the mass spectrum (Fig. 2a) after gaseous 2-methyl-2-butanol was exposed to 70 wt% H_2SO_4 solution. An alkene likely accounted for this peak as we

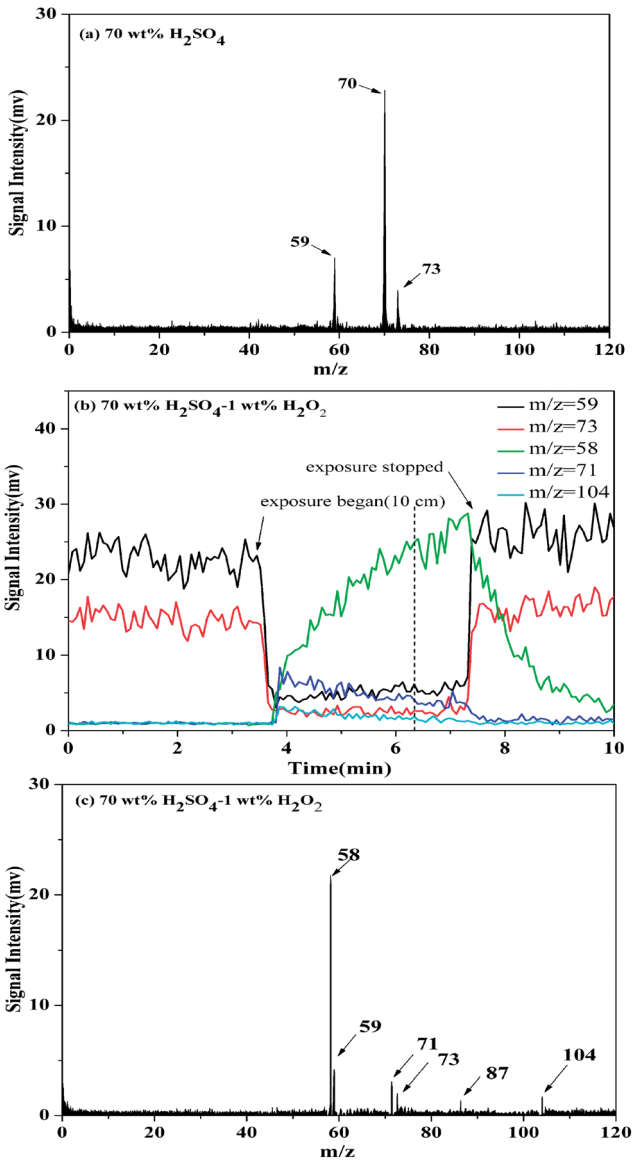

Fig. 2 Typical uptake experimental profiles of 2-methyl-2-butanol. (a) The real-time mass spectrum after gaseous 2-methyl-2-butanol was exposed to 70 wt% H_2SO_4 solution; (b) the profiles of monitoring ion peaks in real-time during the uptake of 2-methyl-2-butanol into 70 wt % H_2SO_4–1 wt% H_2O_2 mixed solution; (c) real-time mass spectrum at the time marked by dash line in (b). The peak at m/z = 87 is not shown in (b) because the SPI-TOFMS can only monitor five peaks at one time.

found evident resemblance between the gas-phase product IR (Fig. S2d†) and reference 2-methyl-2-butene IR. Based on the aqueous-phase products analysis, the peak at $m/z = 167$ ($C_5H_{11}SO_4^-$) in Fig. S3b† is due to the generation of organosulfates. These results suggest that organosulfates and alkene are created by the heterogeneous interactions.

In contrast to the uptake of 2-methyl-2-butanol on H_2SO_4, obvious changes appeared when adding H_2O_2 into H_2SO_4 solution. As shown in Fig. 2b and c, 2-methyl-2-butanol signals ($m/z = 59$ and 73) dropped down meanwhile four new peaks at $m/z = 58$, 71, 87 and 104 appeared after the gaseous reactant was exposed to 70 wt% H_2SO_4–1 wt% H_2O_2 mixed solution. Evident changes also appear in the IR spectrum of gas-phase product (Fig. S4b†), the band at 1740 cm^{-1} is deduced to belong to a C=O stretch. In the light of these results, the peak at $m/z = 58$ detected in the mass spectrum is attributed to the molecule ion of acetone. The peak at $m/z = 71$ ($C_5H_{11}^+$) is deduced to be a fragment of *tert*-amyl hydroperoxide (TAHP) according to following experimental evidences. A similar peak was also detected in our previous study on the uptake of MBO into H_2SO_4–H_2O_2 mixed solution:[39] in that paper, a new peak at $m/z = 69$ was observed through heterogeneous reactions and was ascribed to an online-product which needed to be further identified. The peaks at $m/z = 87$ and 104 likely stand for TAHP fragment and TAHP molecular ion, respectively. To further investigate this reaction pathway, a series of experiments of aqueous-phase reactions were performed. Fig. S5a† shows the gas chromatogram of the extracted organic-phase from aqueous-phase reactions of 2-methyl-2-butanol and H_2SO_4 (pH = 1)–H_2O_2 (300 mM) mixed solution. Peaks 1–4 in the chromatogram correspond to butane, acetone, solvent dichloromethane and reactant 2-methyl-2-butanol, respectively, all of these mass spectra match excellently with those from the MS library. Due to the lack of mass spectra of possible products (TAHP and di-*tert*-amyl peroxide (DTAP)) in the MS library, liquid TAHP and DTAP were injected into GC-MS to obtain the corresponding mass spectra. Additionally, aqueous-phase reactions of *tert*-butyl alcohol and H_2SO_4–H_2O_2 mixed solution were also performed in the same experimental conditions because of the similar structure of these two compounds, the products were identified using GC-MS. Therefore, we infer that peak 5 and 6 in Fig. S5a† belongs to TAHP and DTAP signals respectively for several reasons: (i) mass spectrum of peak 5 in Fig. S5a† is nearly the same as that of TAHP, obvious resemblance is also found between the mass spectrum of peak 6 and that of DTAP. (ii) According to the GC-MS results, *tert*-butyl hydroperoxide and di-*tert*-butyl peroxide are found to be produced during the aqueous-phase reactions of *tert*-butyl alcohol and H_2SO_4–H_2O_2 mixed solution. Considering the similar structure of 2-methyl-2-butanol and *tert*-butyl alcohol, ROOH maybe also formed from the reaction of 2-methyl-2-butanol and H_2SO_4–H_2O_2 mixed solution. (iii) In the realm of organic chemistry, TAHP and DTAP could be synthesized by the reaction of *tert*-amyl alcohol and H_2SO_4–H_2O_2 mixed solution, which was under very strict control.[40] (iv) Acetone and butane provide an indirect evidence for the formation of DTAP because they are suggested to be the main pyrolysis products of DTAP at 523 K (see Fig. S6a† for detailed mechanism).[40] Considering the inlet temperature of GC-MS was set at 523 K, acetone and butane might be formed through this pathway. TAHP and DTAP were also generated in H_2SO_4 (pH = 1)–H_2O_2 (10 mM) mixed solution (see Fig. S5b†).

Compared to the aqueous-phase reactions between 2-methyl-2-butanol and H_2SO_4, a new peak at $m/z = 183$ ($C_5H_{11}SO_5^-$) appeared in the ESI-MS spectrum of extracted organic-phase from the reaction between 2-methyl-2-butanol and H_2SO_4–H_2O_2 mixed solution (Fig. S3c†). This peak was inferred to be related to *tert*-amyl hydrogen peroxysulfate (TAPS), which was produced by the reaction of TAHP and H_2SO_4. In order to confirm our hypothesis, both the uptake of gaseous TAHP on H_2SO_4 solution and the aqueous-phase reactions between TAHP and H_2SO_4 were conducted. The same peak at $m/z = 183$ obtained from the ESI-MS (Fig. S3d†) was also found during the aqueous-phase reactions of TAHP and H_2SO_4. Fig. 3a depicts the mass spectrum of TAHP and five peaks ($m/z = 58$, 59, 71, 87 and 104) are observed. These peaks have a good agreement with the peaks shown in Fig. 2c. Exposing gaseous THAP to H_2SO_4 (Fig. 3b) led to an increment of the signal intensity for the peak at $m/z = 58$ while other peaks dropped to a certain extent at the same time. Although the peak at $m/z = 58$ is one of fragments of TAHP, we suppose acetone makes a main contribution to peak at $m/z = 58$ in Fig. 2c for three reasons: (i) the peak at $m/z = 58$ in Fig. 2c is the strongest fragment, which can hardly caused only by the fragment of TAHP according to the relative peak intensity between the molecular ion peak at $m/z = 104$ and fragment peak at $m/z = 58$ (shown in Fig. 3a). (ii) Fig. S4d† shows the IR spectrum of products formed in the heterogeneous reaction of TAHP and H_2SO_4, the band around 1740 cm^{-1} allows a straightforward detection of C=O stretching modes. This result gives a strong support to the formation of carbonyl compounds. (iii) Acetone may be formed through the protolytic cleavage-rearrangement reactions of TAHP in acidic media according to previous work.[41] Based on all these experimental evidences, TAHP, DTAP, TAPS and acetone are considered to be generated by the heterogeneous reactions of 2-methyl-2-butanol and H_2SO_4–H_2O_2 mixed solution. Detailed reaction mechanism is discussed in the subsequent section.

As for the uptake of 3-buten-2-ol in H_2SO_4 solution (Fig. 3c), the reactant signals ($m/z = 43$, 57 and 72) decreased quickly after gaseous 3-buten-2-ol was exposed to H_2SO_4, simultaneously a new peak at $m/z = 54$ appeared. Similar to the uptake of former two alcohols, this peak is caused by an alkene because the product IR (Fig. S2f†) is nearly the same as the reference 1,3-butadiene IR. In the light of ESI-MS result (Fig. S3e†), the peak at $m/z = 151$ ($C_4H_7SO_4^-$) is inferred to be 1-methylallyl sulfate signal, just like the reactions of former two alcohols and H_2SO_4.

Fig. 3e shows the temporal profiles of all ion peaks during the uptake of 3-buten-2-ol into 70 wt% H_2SO_4–1 wt% H_2O_2 mixed solution, and Fig. 3f is the real-time mass spectrum after exposure. The 3-buten-2-ol signals dropped down as soon as the reaction started and two new peaks at $m/z = 44$ and 55 appeared. The peak at $m/z = 55$ ($C_4H_7^+$) is 1 amu larger than the dehydration product 1,3-butadiene. The similar cases also occurred in the uptake experiments of MBO and 2-methyl-2-butanol.[39]

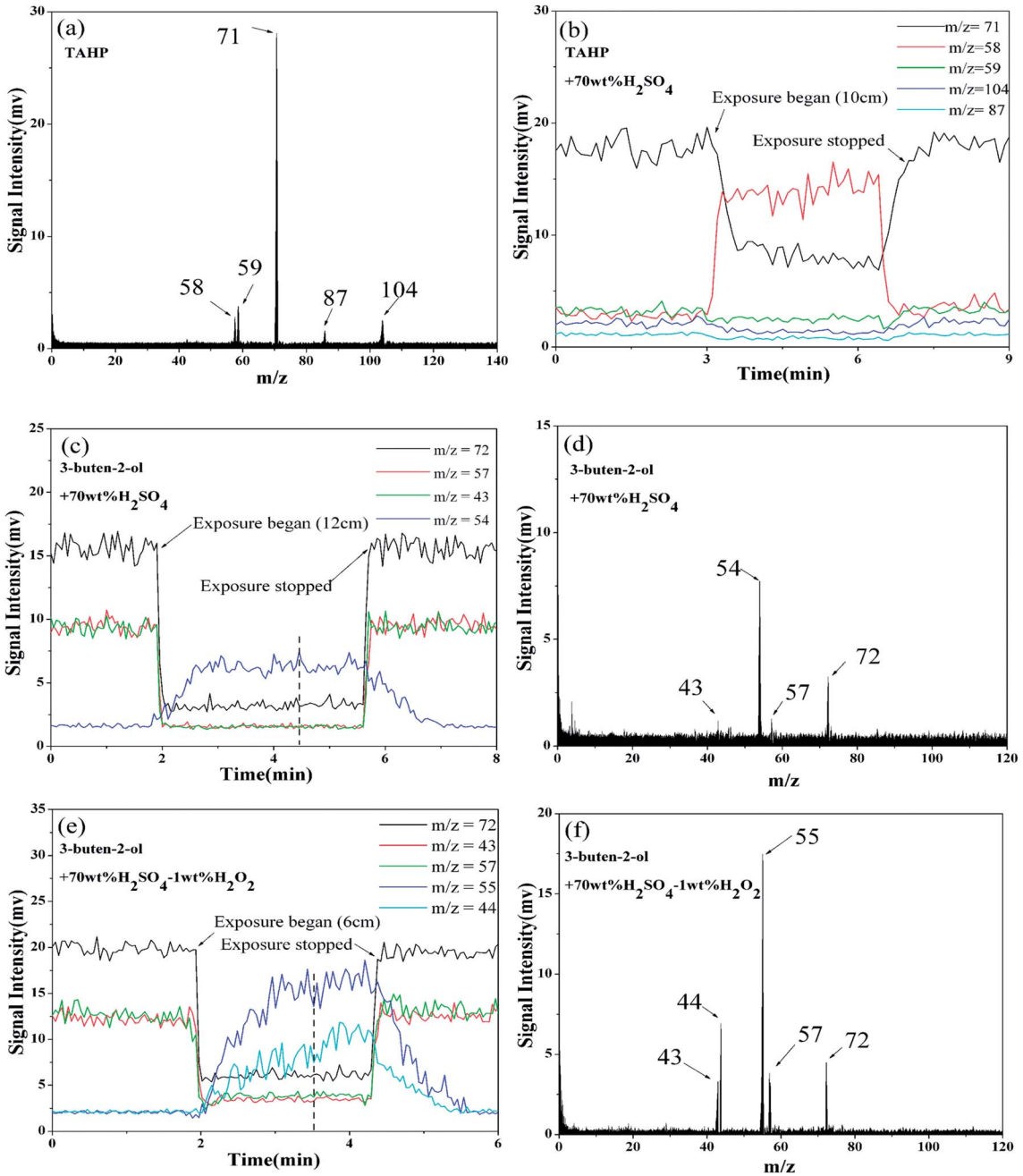

Fig. 3 Typical experimental profiles of TAHP and 3-buten-2-ol. (a) The vacuum UV mass spectra of TAHP. (b) The profiles of monitoring all ion peaks in real-time during the uptake of TAHP into 70 wt% H_2SO_4 solution. (c) The profiles of monitoring all ion peaks in real-time during the uptake of 3-buten-2-ol into 70 wt% H_2SO_4 solution. (d) Real-time mass spectrum at the time marked by dash line in (c). (e) The profiles of monitoring all ion peaks in real-time during the uptake of 3-buten-2-ol into 70 wt% H_2SO_4–1 wt% H_2O_2 mixed solution. (f) Real-time mass spectrum at the time marked by dash line in (e).

Consequently, we infer methylallyl hydroperoxide (MAHP) is generated by this heterogeneous reaction and the peak at $m/z =$ 55 is one of its fragments. As shown in Fig. S4f,† a strong band around 1745 cm^{-1} is observed in gas-phase products, which should be caused by carbonyl compounds. On the basis of these results, the peak at $m/z = 44$ in Fig. 3f is inferred to belong to the molecular ion of acetaldehyde. The reaction pathway is discussed in detail in the following section. Due to the lack of standard compound, the information about the mass spectrum of MAHP is limited and the aqueous-phase products were only analyzed by ESI-MS. As mentioned above, organic hydrogen peroxysulfate ($ROOSO_3H$) is created by the reaction of ROOH and H_2SO_4. Therefore, if MAHP was formed in the aqueous-phase reactions, $ROOSO_3H$ should be detected by ESI-MS. The peak at $m/z = 167$ ($C_4H_7SO_5^-$) (Fig. S3f†) is deduced to be 1-methylallyl hydrogen peroxysulfate signal. These results reveal that ROOH are also formed through the acid-catalyzed oxidation of 3-buten2-ol with H_2O_2.

Reaction mechanism

As stated above, TAHP, DTAP, TAPS and acetone are considered to be produced by the heterogeneous reactions of 2-methyl-2-butanol and H_2SO_4–H_2O_2 mixed solution. Combining the results obtained from SPI-TOFMS, FTIR spectrometer, GC-MS, ESI-MS and previous research,[40] the proposed chemical mechanism for the formation and degradation of TAHP is shown in Fig. 4. The initial step involves the addition of a proton to the hydroxyl of 2-methyl-2-butanol followed by the elimination of H_2O and generation of tertiary carbocations. Based on the previous studies, ROOH may be prepared by nucleophilic attack of concentrated H_2O_2 on carbonium ions and the reaction is proposed to follow an S_N1 pathway.[38,41] Considering HO_2^- (caused by heterolysis of H_2O_2) is a strong nucleophile, the possible ROOH formation mechanism is HO_2^- attack the carbocations. Thus, HO_2^- or hydrogen sulfate ion (HSO_4^-) could attack carbocations in the following step, giving TAHP and organosulfates, respectively. In the realm of organic chemistry, TAHP was synthesized based on the method introduced by Milas and Surgenor:[40] adding concentrated H_2O_2 into *tert*-amyl sulfate (TAS) solution (prepared by reaction of 2-methyl-2-butanol and H_2SO_4) could lead to the generation of TAHP (main product) and DTAP (byproduct). Under this condition, HO_2^- or OH^- may attack different positions of TAS, thus producing TAHP. To the best of our knowledge, in previous literature little attention was paid to the question that which route might be the main pathway. To get a better understanding of the chemical mechanism, two experiments are designed: the first one is adding $H_2{}^{18}O_2$ into TAS, the other one is adding 2-methyl-2-butanol into mixed H_2SO_4–$H_2{}^{18}O_2$ solution. As shown in Fig. 4, if HO_2^- pathway is the main route, TAHP formed by this way will further react with H_2SO_4, thus a peak at m/z = 185 ($C_5H_{11}S^{16}O_4{}^{18}O^-$) should be detected by ESI-MS. Conversely, if OH^- pathway controls the reaction, a peak at m/z = 183 ($C_5H_{11}S^{16}O_5^-$) should be found. Referring to Fig. S3g and h,† the peak at m/z = 167 is attributed to TAS and the peak at m/z = 185 represents the $ROOSO_3H$ formed though HO_2^- route. Weak peaks at m/z = 183 were also detected, this might be due to the OH^- pathway or the influence of $H_2{}^{18}O_2$ (contain 10 atom% ^{16}O). Considering the strong intensity of the peak at m/z = 185, we conclude that HO_2^- route is the main pathway.

Once generated in H_2SO_4 solution, the degradation of TAHP occurs simultaneously. On one hand, cleavage of oxygen to oxygen (O–O) bond in TAHP produces alkoxyl radicals (RO), which then react further with H_2SO_4 to produce TAPS or combine with other RO to form DTAP. On the other hand, TAHP undergoes an acid-catalyzed rearrangement which leads to the formation of acetone. Fig. 5 depicts the rearrangement mechanism. The cleavage of O–O bond of conjugate acid, caused by the protonation at oxygen atom, leads to the formation of a highly energetic oxenium ion. Then the oxenium ion rearranges to the alkylated ketone immediately, which reacts further to produce acetone and ethanol. The relative migratory ability of different groups follows the trend ethyl > methyl during the rearrangement. Although magic acid (not H_2SO_4) was used in the study of rearrangement of ROOH in previous research,[41] we thought this process could also take place in the presence of H_2SO_4 because it was reported that *tert*-butyl hydroperoxide underwent a similar rearrangement reaction in H_2SO_4.[42] Ethanol is a missing product of the rearrangement process in our study for two reasons: (i) ethanol tends to stay in the aqueous-phase for its great solubility in water and reacts further with H_2SO_4 to form ethyl sulfate, the similar route is also reported in former paper.[42] (ii) Even though gaseous ethanol is produced, the SPI-TOFMS can hardly detect it because our instrument can only detect species whose ionization energy is below 10.5 eV. Fortunately, according to the products analysis of aqueous-phase reactions between TAHP and H_2SO_4, the peak at m/z = 125 ($C_2H_5SO_4^-$) (Fig. S3d†) which is ascribed to ethyl sulfate, gives an indirect evidence for the generation of ethanol.

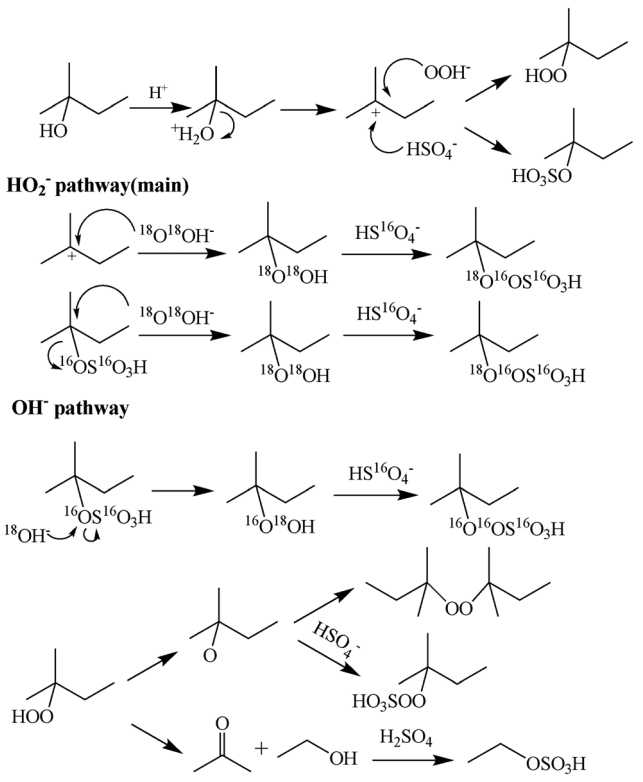

Fig. 4 Proposed chemical mechanism for the formation of TAHP during the heterogeneous acid-catalyzed oxidation of 2-methyl-2-butanol with H_2O_2.

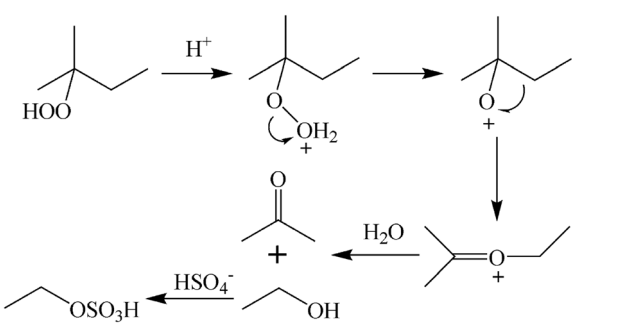

Fig. 5 Proposed chemical mechanism for the acid-catalyzed rearrangement of TAHP.

Moreover, when extending the formation mechanism of ROOH to our previous work,[39] it is logical to infer that 1,1-dimethylallyl hydroperoxide is generated by the uptake of MBO into H_2SO_4–H_2O_2 mixed solution. If ROOH formed from MBO undergoes the same rearrangement mechanism just as TAHP does, acetone and acetaldehyde should be the products (see Fig. S6b† for detailed mechanism). Previous results have shown a good agreement with our conjecture. Considering all this, it is reasonable to conclude that TAHP undergoes a rearrangement reaction in H_2SO_4.

As for the chemical mechanism during the reaction of 3-buten-2-ol and H_2SO_4–H_2O_2 mixed solution, ROOH is also formed and follows the same rule as 2-methyl-2-butanol undergoes (see Fig. S6c† for detailed information). Experimental evidence is limited to validate the generation of ROOR, nevertheless, it is a possible route for the formation of methylallyl peroxide during the heterogeneous interaction as DTAP is produced under the similar condition. It is very interesting that H_2O_2 changes the chemical mechanism of 2-methyl-2-butanol and 3-buten-2-ol, while it has no obvious effect on 2-butanol, leading to a higher γ for 2-methyl-2-butanol and 3-buten-2-ol. The different reactivity may be caused by the stability of carbocations formed during the reactions: more stable carbocations may contribute to the generation of ROOH while the less stable carbocations may not. Our results are consistent with previous findings.[43]

Conclusion and atmospheric implications

In this work, the γ of three different structures of ROH into H_2SO_4–H_2O_2 mixed solution were calculated and the corresponding chemical pathways were deduced according to the products information. For 2-methyl-2-butanol and 3-buten-2-ol, ROOH, ROOR, $ROOSO_3H$ and organosulfates were found to be created by the heterogeneous interactions. The newly found acid-catalyzed pathway may provide a potential route for ROOH formation and influence particle growth.

It has been suggested that the majority of the ROOH in the gas-phase are formed *via* the recombination reaction of HO_2 and RO_2 during the daytime.[9] Other mechanisms for the formation of ROOH in the absence of light include the ozonolysis reaction of alkenes[9,10] and aqueous-phase reaction between H_2O_2 and aldehydes.[11] Here, we introduce another possible pathway for the formation of ROOH during the acid-catalyzed oxidation of ROH (limited to tertiary or allyl alcohols) with H_2O_2. Tertiary and allyl aliphatic alcohols are emitted into the atmosphere by different natural and anthropogenic sources. For example, a series of tertiary and allyl alcohols are emitted to the atmosphere by plant species,[13] MBO can be highly abundant in pine forests of the western United States,[14–16] 3-methyl-2-buten-1-ol is an ingredient used in fine fragrances with production of 1–10 metric tons per year.[44] Hence, considering the high concentration of total release of tertiary and allyl alcohols by pine forests, they may contribute to ROOH formation through the acid-catalyzed reactions. However, only short-chain ($C \leq 2$) ROOH (mainly MHP, EHP and HMHP) have been measured in the environment in the past two decades.[6–8] According to the review summarized by Reeves and Penkett,[45] high performance liquid-phase chromatography with post-column enzyme derivatization is a useful method to detect individual ROOH. Horseradish peroxidase (HRP) was used to catalyze the reduction of ROOH in previous field measurements.[6–8,46,47] It should be pointed out that HRP can only effectively catalyze the reduction of H_2O_2 and short-chain ($C \leq 2$) ROOH because of its specificity for the hydrogen receptor.[48] Furthermore, many standards of long-chain ROOH (for example, 1,1-dimethylallyl hydroperoxide) are not available. These two factors may inhibit the measurement of ROOH formed through the acid-catalyzed pathway. Based on the experimental evidence (2-methyltetrols was found to be produced by the reaction of isoprene and H_2SO_4–H_2O_2 mixed solution) and field measurements, Claeys *et al.* suggested that multiphase acid-catalyzed oxidation of isoprene with H_2O_2 may contribute to SOA formation.[24] Similarly, on the basis of the aqueous-phase reaction results shown in the present work, it seems logical to assume that the acid-catalyzed reactions of ROH may also occur under certain conditions and contribute to ROOH formation. Our results imply that this acid-catalyzed route is a potential source for ROOH formation and more research is needed to elucidate the role of this pathway.

The heterogeneous reactions may influence particle growth, especially in the upper troposphere where sulfate aerosols are more concentrated. Organosulfates were deduced to be produced during the acid-catalyzed reactions. They were reported to undergo a slow hydrolysis reaction and likely to be stable during the lifetime of most ambient SOA.[49,50] The uptake of ROH into existing acidic particles could lead to the formation of low-volatility organosulfates, which tend to stay stable in the particle-phase and contribute to the particles growth. In addition, aldehydes and ketones are found to be generated by the acid-catalyzed rearrangement reaction of ROOH. These carbonyl compounds may undergo aldol condensation and polymerization in the acidic media,[3,51] thus leading to the formation of higher-molecule weight compounds which may also make a contribution to the particle growth for their low volatility.

Acknowledgements

This research was financially supported by the Strategic Priority Research Program (B) of the Chinese Academy of Sciences (XDB05010400) and National Natural Science Foundation of China (Major Program: 21190052 & Contract no. 41173112, 21077109,40925016).

References

1 J. G. Calvert, A. Lazrus, G. L. Kok, B. G. Heikes, J. G. Walega, J. Lind and C. A. Cantrell, *Nature*, 1985, **317**, 27–35.
2 F. Ravetta, D. J. Jacob, W. H. Brune, B. G. Heikes, B. E. Anderson, D. R. Blake, G. L. Gregory, G. W. Sachse, S. T. Sandholm, R. E. Shetter, H. B. Singh and R. W. Talbot, *J. Geophys. Res.*, 2001, **106**, 32709–32716.
3 M. Hallquist, J. C. Wenger, U. Baltensperger, Y. Rudich, D. Simpson, M. Claeys, J. Dommen, N. M. Donahue,

C. George, A. H. Goldstein, J. F. Hamilton, H. Herrmann, T. Hoffmann, Y. Iinuma, M. Jang, M. E. Jenkin, J. L. Jimenez, A. Kiendler-Scharr, W. Maenhaut, G. McFiggans, T. F. Mentel, A. Monod, A. S. H. Prevot, J. H. Seinfeld, J. D. Surratt, R. Szmigielski and J. Wildt, *Atmos. Chem. Phys.*, 2009, **9**, 5155–5236.

4 Q. Chen, Y. J. Liu, N. M. Donahue, J. E. Shilling and S. T. Martin, *Environ. Sci. Technol.*, 2011, **45**, 4763–4770.

5 C. N. Hewitt, G. L. Kok and R. Fall, *Nature*, 1990, **344**, 56–58.

6 E. Hellpointner and S. Gab, *Nature*, 1989, **337**, 631–634.

7 C. N. Hewitt and G. L. Kok, *J. Atmos. Chem.*, 1991, **12**, 181–194.

8 J. Valverde-Canossa, W. Wieprecht, K. Acker and G. K. Moortgat, *Atmos. Environ.*, 2005, **39**, 4279–4290.

9 K. H. Becker, K. J. Brockmann and J. Bechara, *Nature*, 1990, **346**, 256–258.

10 M. H. Lee, B. G. Heikes and D. W. O'Sullivan, *Atmos. Environ.*, 2000, **34**, 3475–3494.

11 R. Zhao, A. K. Y. Lee, R. Soong, A. J. Simpson and J. P. D. Abbatt, *Atmos. Chem. Phys.*, 2013, **13**, 5857–5872.

12 P. D. Goldan, W. C. Kuster, F. C. Fehsenfeld and S. A. Montzka, *Geophys. Res. Lett.*, 1993, **20**, 1039–1042.

13 G. Konig, M. Brunda, H. Puxbaum, C. N. Hewitt, S. C. Duckham and J. Rudolph, *Atmos. Environ.*, 1995, **29**, 861–874.

14 P. Harley, V. Fridd-Stroud, J. Greenberg, A. Guenther and P. Vasconcellos, *J. Geophys. Res.*, 1998, **103**, 25479–25486.

15 M. S. Lamanna and A. H. Goldstein, *J. Geophys. Res.*, 1999, **104**, 21247–21262.

16 N. C. Bouvier-Brown, A. H. Goldstein, D. R. Worton, D. M. Matross, J. B. Gilman, W. C. Kuster, D. Welsh-Bon, C. Warneke, J. A. de Gouw, T. M. Cahill and R. Holzinger, *Atmos. Chem. Phys.*, 2009, **9**, 2061–2074.

17 A. V. Jackson, *Crit. Rev. Environ. Sci. Technol.*, 1999, **29**, 175–228.

18 D. J. Straub, T. Lee and J. L. Collett, *J. Geophys. Res.*, 2007, **112**, D04307.

19 A. S. Hasson and S. E. Paulson, *J. Aerosol Sci.*, 2003, **34**, 459–468.

20 C. Arellanes, S. E. Paulson, P. M. Fine and C. Sioutas, *Environ. Sci. Technol.*, 2006, **40**, 4859–4866.

21 J. D. Surratt, Y. Gomez-Gonzalez, A. W. H. Chan, R. Vermeylen, M. Shahgholi, T. E. Kleindienst, E. O. Edney, J. H. Offenberg, M. Lewandowski, M. Jaoui, W. Maenhaut, M. Claeys, R. C. Flagan and J. H. Seinfeld, *J. Phys. Chem. A*, 2008, **112**, 8345–8378.

22 J. D. Surratt, A. W. H. Chan, N. C. Eddingsaas, M. N. Chan, C. L. Loza, A. J. Kwan, S. P. Hersey, R. C. Flagan, P. O. Wennberg and J. H. Seinfeld, *Proc. Natl. Acad. Sci. U. S. A.*, 2010, **107**, 6640–6645.

23 L. E. Hatch, J. M. Creamean, A. P. Ault, J. D. Surratt, M. N. Chan, J. H. Seinfeld, E. S. Edgerton, Y. X. Su and K. A. Prather, *Environ. Sci. Technol.*, 2011, **45**, 5105–5111.

24 M. Claeys, W. Wang, A. C. Ion, I. Kourtchev, A. Gelencser and W. Maenhaut, *Atmos. Environ.*, 2004, **38**, 4093–4098.

25 O. Boge, Y. Miao, A. Plewka and H. Herrmann, *Atmos. Environ.*, 2006, **40**, 2501–2509.

26 J. Guo, Y. Wang, X. H. Shen, Z. Wang, T. Lee, X. F. Wang, P. H. Li, M. H. Sun, J. L. Collett, W. X. Wang and T. Wang, *Atmos. Environ.*, 2012, **60**, 467–476.

27 E. Harris, B. Sinha, D. van Pinxteren, A. Tilgner, K. W. Fomba, J. Schneider, A. Roth, T. Gnauk, B. Fahlbusch, S. Mertes, T. Lee, J. Collett, S. Foley, S. Borrmann, P. Hoppe and H. Herrmann, *Science*, 2013, **340**, 727–730.

28 R. J. Ferek, A. L. Lazrus, P. L. Haagenson and J. W. Winchester, *Environ. Sci. Technol.*, 1983, **17**, 315–324.

29 S. M. Kane and M. T. Leu, *J. Phys. Chem. A*, 2001, **105**, 1411–1415.

30 N. P. Levitt, J. Zhao and R. Y. Zhang, *J. Phys. Chem. A*, 2006, **110**, 13215–13220.

31 B. Noziere, D. Voisin, C. A. Longfellow, H. Friedli, B. E. Henry and D. R. Hanson, *J. Phys. Chem. A*, 2006, **110**, 2387–2395.

32 L. L. Van Loon and H. C. Allen, *J. Phys. Chem. A*, 2008, **112**, 7873–7880.

33 T. H. Wang, Z. Liu, W. G. Wang and M. F. Ge, *Atmos. Environ.*, 2012, **56**, 58–64.

34 D. M. Murphy and D. W. Fahey, *Anal. Chem.*, 1987, **59**, 2753–2759.

35 D. R. Hanson, J. B. Burkholder, C. J. Howard and A. R. Ravishankara, *J. Phys. Chem.*, 1992, **96**, 4979–4985.

36 E. N. Fuller, P. D. Schettler and J. C. Giddings, *Ind. Eng. Chem. Res.*, 1966, **58**, 19–27.

37 P. Davidovits, C. E. Kolb, L. R. Williams, J. T. Jayne and D. R. Worsnop, *Chem. Rev.*, 2006, **106**, 1323–1354.

38 A. G. Davies, R. V. Foster and A. M. White, *J. Chem. Soc.*, 1953, 1541–1547.

39 Z. Liu, M. F. Ge, W. G. Wang, S. Yin and S. R. Tong, *Phys. Chem. Chem. Phys.*, 2011, **13**, 2069–2075.

40 N. A. Milas and D. M. Surgenor, *J. Am. Chem. Soc.*, 1946, **68**, 643–644.

41 G. A. Olah, D. G. Parker, N. Yoneda and F. Pelizza, *J. Am. Chem. Soc.*, 1976, **98**, 2245–2250.

42 N. C. Deno, W. E. Billups, K. E. Kramer and R. R. Lastomir, *J. Org. Chem.*, 1970, **35**(9), 3080–3082.

43 R. Criegee and H. Dietrich, *Liebigs Ann. Chem.*, 1948, **560**, 135–141.

44 D. McGinty, L. Jones, C. S. Letizia and A. M. Api, *Food Chem. Toxicol.*, 2010, **48**, S64–S69.

45 C. E. Reeves and S. A. Penkett, *Chem. Rev.*, 2003, **103**, 5199–5218.

46 Y. Ren, A. J. Ding, T. Wang, X. H. Shen, J. Guo, J. M. Zhang, Y. Wang, P. J. Xu, X. F. Wang, J. Gao and J. L. Collett, *Atmos. Environ.*, 2009, **43**, 1702–1711.

47 R. B. Morgan and A. V. Jackson, *J. Geophys. Res.*, 2002, **107**, D19.

48 G. G. Guilbault, *Handbook of Enzymatic Methods of Analysis*, Marcel Dekker, New York, 1976.

49 K. S. Hu, A. I. Darer and M. J. Elrod, *Atmos. Chem. Phys.*, 2011, **11**, 8307–8320.

50 A. I. Darer, N. C. Cole-Filipiak, A. E. O'Connor and M. J. Elrod, *Environ. Sci. Technol.*, 2011, **45**, 1895–1902.

51 M. S. Jang, N. M. Czoschke, S. Lee and R. M. Kamens, *Science*, 2002, **298**, 814–817.

